Available online at www.sciencedirect.com
SCIENCE DIRECT®
Journal of Magnetic Resonance 168 (2004) 8–17
JMR Journal of Magnetic Resonance
www.elsevier.com/locate/jmr

Towards quantitative measurements in solid-state CPMAS NMR: A Lee–Goldburg frequency modulated cross-polarization scheme

Riqiang Fu,[a,*] Jun Hu,[a,b] and Timothy A. Cross[a,b,c]

[a] *Center for Interdisciplinary Magnetic Resonance, National High Magnetic Field Laboratory, 1800 E. Paul Dirac Drive, Tallahassee, FL 32310, USA*
[b] *Department of Chemistry and Biochemistry, Florida State University, Tallahassee, FL 32306, USA*
[c] *Institute of Molecular Biophysics, Florida State University, Tallahassee, FL 32306, USA*

Received 11 September 2003; revised 13 January 2004

Abstract

A new scheme combining a Lee–Goldburg (LG) sequence with frequency modulation is proposed for cross-polarization (LG-FMCP) in solid-state magic-angle-spinning nuclear magnetic resonance. During the CP contact time, the ^{1}H magnetization is spin-locked along the magic angle by the LG sequence and the irradiation offset of the S spins (e.g., ^{15}N) is modulated sinusoidally with a constant RF amplitude. It is shown experimentally that the LG sequence significantly lengthens the proton spin–lattice relaxation time in the tilted rotating frame and that the frequency modulation shortens the cross-polarization time for non-protonated S spins. As a result of substantially increasing the difference in these relaxation rates, the non-protonated and protonated S spins can be more efficiently and more uniformly polarized with a relatively long CP contact time, making quantitative CP measurements possible. A sample of ^{15}N-δ_1-L-histidine lyophilized from a solution of pH 6.3 and a ^{15}N-δ_1-L-His labeled transmembrane helical peptide in hydrated lipid bilayers were used to illustrate the advantages of this scheme.

Keywords: NMR; Frequency modulated cross-polarization; Lee–Goldburg sequence; Magic angle spinning; Histidine; M2 protein

1. Introduction

Relaxation parameters too often represent the "intrinsic" property of the sample for which there is nothing that can be done. They dictate line-widths, recycle delays, polarization transfer rates, etc. A few mechanisms over the years have been developed to modify these rates such as partial deuteration of proteins [1,2]. Alternatively, there are a few examples where different relaxation rates have been substituted for ones with poor properties such as PISEMA [3]. Cross-polarization (CP) [4], which dramatically enhances the polarization of dilute nuclei, S with low gyromagnetic ratios from abundant nuclei, I with higher gyromagnetic ratios, is an example where recycle delays are no longer dependent on T_1^S but on T_1^H. These spin–lattice relaxation times for the S and I spins typically have values where T_1^S is much longer than T_1^H. However, one of the long-standing problems with quantitation of CP has been the competition between T_{IS} and $T_{1\rho}^H$ during polarization transfer, where T_{IS} and $T_{1\rho}^H$ represent the cross-polarization time and proton spin–lattice relaxation time in the rotating frame, respectively. If these rates are quite similar, intensities for sites having different T_{IS} values will not be comparable. Here, a mechanism for lengthening $T_{1\rho}^H$ is used so that both uniform and increased spectral intensities are achieved.

CP transfer [4] is generally achieved by spin-locking both the I and S spins with radio-frequency (RF) amplitudes that fulfill the Hartmann–Hahn match condition $\Delta = \omega_{1I} - \omega_{1S} = n\omega_r$ [5–7], where ω_r is the spinning frequency and n an integer, while ω_{1I} and ω_{1S} refer to the amplitudes of the RF fields applied to the I and S spins, respectively. Spin dynamics of CP has been extensively analyzed [5,8–11]. In general, the rate of polarization buildup of the S spins can be characterized by T_{IS} and $T_{1\rho}^H$, provided that the spin–lattice relaxation time in the rotating frame for the dilute

* Corresponding author. Fax: 1-850-644-1366.
E-mail address: rfu@magnet.fsu.edu (R. Fu).

1090-7807/$ - see front matter © 2004 Elsevier Inc. All rights reserved.
doi:10.1016/j.jmr.2004.01.012

spins ($T_{1\rho}^{S}$) is so long that it does not affect the CP dynamics. T_{IS} is primarily governed by the strength of the *I*–*S* heteronuclear coupling and represents the polarization buildup process, while $T_{1\rho}^{H}$ is determined by spin diffusion among protons and characterizes the ^{1}H polarization decay in the rotating frame (or spin-lock). For *S* spins directly attached to protons such as ^{15}N–H, -^{13}CH, and -^{13}CH$_2$, the *I*–*S* dipolar coupling is strong and thus gives rise to a very short T_{IS}, resulting in a fast polarization buildup of the *S* spins. On the other hand, for *S* spins that are not directly attached to protons (e.g., non-protonated ^{15}N spins) or whose structural group experiences significant motion (e.g., -CH$_3$), the *I*–*S* dipolar coupling becomes relatively weak resulting in a rather long T_{IS} and thus a slow polarization buildup of the *S* spins. Other factors may also affect the polarization buildup, for instance, any Hartmann–Hahn mismatch Δ may slow the polarization buildup [10], and molecular motions may affect CP dynamics in various ways [12]. Within molecules, there usually exist different bonding structures for the dilute spins, such as protonated and non-protonated *S* spins. Since the CP spin dynamics is the result of competing effects between T_{IS} and $T_{1\rho}^{H}$, it is almost impossible to uniformly polarize all the *S* spins within a molecule at any specific contact time, due to the very different polarization buildup and proton decay rates. Therefore, it is difficult to make quantitative analyses from the resulting CP spectrum, although these features can be very important. For example, $T_{1\rho}^{H}$ filtering experiments [13,14] have been used to separate amorphous (short $T_{1\rho}^{H}$) and crystalline phases (much longer $T_{1\rho}^{H}$) in polymers.

A common approach for quantitative analyses from CP spectra is to perform variable contact time CP experiments [11]. These experiments have been intensely used to analyze quantitative features of coals [15,16]. In spin systems with weak *I*–*S* heteronuclear dipolar couplings, such as non-protonated ^{15}N spins, T_{IS} is on the same order as, or even shorter than, $T_{1\rho}^{H}$, which was widely observed in ^{15}N labeled peptides in hydrated lipid bilayers [17] as well as in other system [18,19]. Consequently, the polarization of the *S* spins becomes rather weak at any given contact time. Therefore, an approach to further enhance the sensitivity of the non-protonated S spins and to more uniformly cross-polarize all of the S spins in a molecule at a given contact time is highly desirable.

In this work, we propose a new CP scheme where the ^{1}H magnetization is spin-locked at the magic angle by a Lee–Goldburg sequence and the irradiation offset of the S spins is modulated in a sine wave during the CP contact time. The advantages of this scheme will be demonstrated in the following section by using a ^{15}N-δ_1-histidine sample and a ^{15}N-δ_1-L-His labeled transmembrane helical peptide in hydrated lipid bilayers.

2. Materials and experiments

L-Histidine specifically enriched in ^{15}N at the δ_1 position was purchased from CIL and used to prepare an aqueous solution whose pH value was adjusted to 6.3. A ^{15}N-δ_1-histidine sample for NMR was prepared by lyophilizing the aqueous solution. All NMR measurements were carried out at room temperature on a Bruker DMX300 NMR spectrometer with Larmor frequencies of 300 and 30 MHz for ^{1}H and ^{15}N, respectively. The variation in spinning rates was controlled to within $\pm$3 Hz. In frequency modulation schemes, the ^{15}N irradiation offset, $\Delta\omega_S(t)$ is modulated sinusoidally over the contact time τ_{CP} [20]

$$\Delta\omega_S(t) = \omega_\Delta \sin(2\pi t/\tau_{CP}), \quad (1)$$

where, ω_Δ is the depth of the frequency modulation. In our experiments, we used $\omega_\Delta/2\pi = 50$ kHz. The waveforms for frequency modulation were generated by a C program and transferred to the waveform generator of the NMR console. For the CP experiments, the matching conditions were optimized experimentally by monitoring the ^{15}N NMR signals recorded at a fixed power level for the ^{1}H RF spin-locking field while varying the power level for the ^{15}N RF spin-locking field. For each experiment, 16 scans were used to accumulate the ^{15}N signals and a two-pulse phase-modulation (TPPM) sequence [21] was used for ^{1}H decoupling during the ^{15}N acquisition. A saturated aqueous $^{15}NH_4NO_3$ solution was used as an external ^{15}N chemical shift reference at 0 ppm.

^{15}N-δ_1-His$_{37}$ transmembrane peptide of the M2 protein (M2-TMP) having the sequence of (NH$_2$-Ser$_{22}$-Ser-Asp-Pro-Leu-Val-Val-Ala-Ala$_{30}$-Ser-Ile-Ile-Gly-Ile-Leu-His$_{37}$-Leu-Ile-Leu$_{40}$-Trp-Ile-Leu-Asp-Arg-Leu^{46}-COOH) was chemically synthesized by solid-phase synthesis on an Applied Biosystems 430A Synthesizer. The peptide was purified and examined as described previously [22]. A unoriented sample for solid state NMR was prepared by incorporated the ^{15}N-δ_1-His$_{37}$M2-TMP into DMPC/DMPG liposomes at pH 8.8 through the detergent removal technique as described in the literature [22,23] and then packed into a 7 mm rotor with a sealing cap.

3. Results and discussion

Fig. 1 shows the ^{15}N MAS NMR spectra of the ^{15}N-δ_1-L-histidine sample lyophilized from a solution of pH 6.3. Clearly, there exist two isotropic ^{15}N chemical shifts positioned at 231.0 and 171.8 ppm. As shown in Scheme 1, the histidine sample may have two neutral species (I) and (II) and a cationic species (III). The neutral species are the two tautomeric forms of the histidine [24,25]. The resonance at 231.0 ppm is from the non-protonated

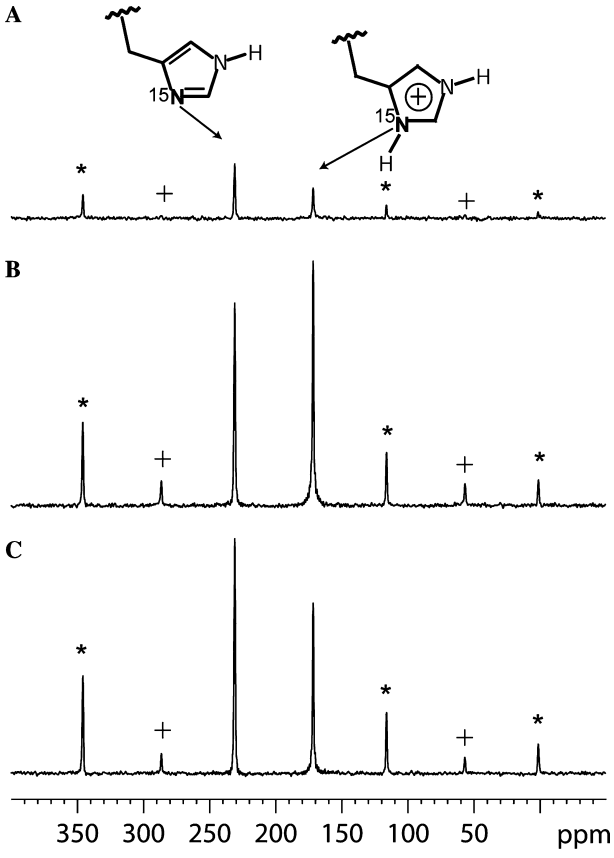

Fig. 1. ^{15}N MAS NMR spectra of the ^{15}N–δ_1-histidine sample obtained using different excitation methods. A Bruker CPMAS NMR probe with 7 mm rotors was used in these experiments. The sample was packed into a 7 mm MAS rotor and was spun at 3.5 kHz during the measurements. (A) A single-pulse excitation (BD) spectrum. A ^{15}N 90° pulse length of 11 μs was used to directly polarize the ^{15}N magnetization with a recycle delay of 7200 s. (B) A cross-polarization (CP) spectrum with a contact time of 2 ms. (C) A CP spectrum with a contact time of 8 ms. A recycle delay of 10 s was used in the CP experiments. The ^{1}H radio-frequency (RF) spin-lock amplitude was set to 27.8 kHz and its CP matched ^{15}N RF spin-lock amplitude was 22.7 kHz. (At such a spinning speed, the CP matching bandwidth was very broad. The ^{15}N RF amplitude used here was the maximum RF amplitude generated by this probe at an input power of ~250 W.) The asterisks and crosses indicate the spinning sidebands of the resonances at 231.0 and 171.8 ppm, respectively.

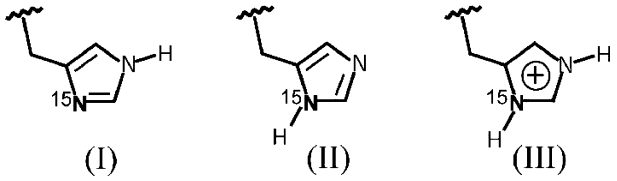

Scheme 1.

^{15}N site and thus assigned to the species (I) [24,26], and the peak at 171.8 ppm is from the protonated ^{15}N site corresponding to the species (III) [26]. No resonance was observed for the species (II), which is consistent with previous observations [24,25]. By using Bloch decay (BD) experiment [27] with a recycle delay of 7200 s (measured ^{15}N T_1 is about 600 s), a quantitative analysis could be made from the spectrum. From Fig. 1A, the ratio of the integrated non-protonated and protonated ^{15}N signal intensities (including all the spinning sidebands) was calculated to be 1.94, implying that the population ratio of species (I) and (III) is 1.94 in the pH 6.3 solution. In conventional continuous-wave cross-polarization (CWCP) experiments, the ^{15}N signals were significantly enhanced compared to that in the BD experiment, as shown in Figs. 1B and C. At a CP contact time of 2 ms, the protonated ^{15}N signal reached its maximum and was enhanced by a factor of 8.1 in comparison to that in Fig. 1A. However, the enhancement factor was only 3.7 for the non-protonated ^{15}N site at that contact time. When the contact time was increased to 8 ms, the protonated ^{15}N signal intensity decreased by 30% clearly indicating the $T_{1\rho}^H$ effect on the polarized ^{15}N signal and the non-protonated ^{15}N signal increased by 16% implying that the effect of the polarization buildup (T_{IS}) was still larger than that of the $T_{1\rho}^H$ decay. The enhancement factors at a contact time of 8 ms became 5.6 and 4.5 for the protonated and non-protonated ^{15}N sites, respectively. This illustrates how difficult it is to quantify CP spectra at any given contact time.

A pulse sequence commonly used for indirect $T_{1\rho}^H$ measurements is diagramed in Fig. 2A. In the beginning of the sequence, the ^{1}H magnetization is rotated from the z-axis to the y-axis in the rotating frame by a 90°

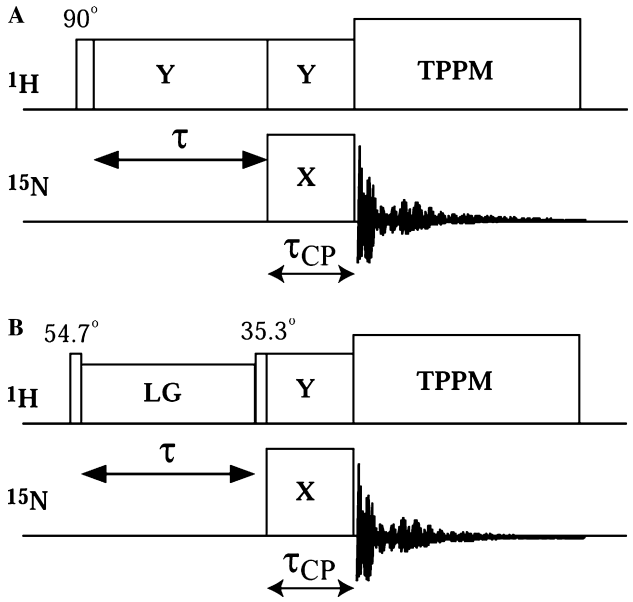

Fig. 2. Pulse sequences used for indirect measurement of proton spin–lattice relaxation times in the rotating frame in different spin lock schemes. (A) Spin lock in the x–y plane by on-resonance continuous-wave (CW) irradiation. (B) Spin lock at the magic angle by a Lee–Goldburg (LG) sequence [28].

pulse and then spin-locked along the y-axis by continuous-wave on-resonance irradiation for a duration of τ. After that, the ^{15}N signals are polarized by CWCP and detected during high power proton decoupling. Consequently, the proton magnetization as a function of spin-lock time τ can be indirectly monitored by the ^{15}N signal intensities. In Fig. 2B, the ^{1}H magnetization is initially flipped to the magic angle by a 54.7° pulse and then spin-locked by a Lee–Goldburg (LG) sequence [28] for the duration of τ. Here, LG refers to an RF pulse with amplitude ω_{1H} applied along the $+y$ direction at an offset of $\Delta\omega_H$ away from the center of the ^{1}H spectrum fulfilling the condition of $\omega_{1H} = \sqrt{2}\Delta\omega_H$. Thus the effective field of the LG sequence lies along the magic angle with an effective spin-lock amplitude of $\sqrt{3/2}\omega_{1H}$. At the end of the spin-lock, a 35.3° pulse rotates the ^{1}H magnetization from the magic angle to the y-axis followed by ^{15}N detection via CWCP. Thus, the proton spin–lattice relaxation time in the tilted rotating frame ($T_{1\rho}^{T,H}$) can be indirectly measured.

Fig. 3 shows the semilog plot of normalized ^{15}N signal intensities versus spin-lock time, τ obtained from the pulse sequences shown in Fig. 2. In these experiments, the sample was packed into a 4 mm MAS rotor and was spun at 6.0 kHz to reduce the sideband intensities. Only the centerband intensities were used for the plot. By fitting the experimental data, it was found that when the ^{1}H magnetization was spin-locked on-resonance the measured $T_{1\rho}^{H}$ was 17.88 and 13.63 ms for the protonated (i.e., the species III) and non-protonated (i.e., the species I) ^{15}N sites, respectively, while $T_{1\rho}^{T,H}$ became 37.40 and 28.92 ms when spin-locked at the magic angle for these sites, respectively. In other words, the spin–lattice relaxation process in the tilted rotating frame is slower by more than a factor of two along the magic angle than in the x–y plane. This phenomenon was observed before [29]. In fact, the on-resonance RF irradiation scales down the proton homonuclear dipolar interaction by 1/2 [30]. The truncated homonuclear dipolar interaction results in decay of the ^{1}H magnetization along the spin-lock field, particularly in the presence of a relatively weak RF irradiation. In our experiments, the RF amplitude used was just 50.0 kHz, comparable to the homonuclear dipolar interaction in the system studied here. On the other hand, the RF field at the magic angle, to the first order, suppresses the strong proton homonuclear dipolar interaction so that the spin-lock field becomes much larger than the internal interactions in the spin system, thus resulting in a slow $T_{1\rho}^{T,H}$ process, even if the effective RF spin-lock amplitude along the magic angle is the same as in the x–y plane. Haeberlen and Waugh [31] theoretically analyzed the two spin-locking situations by using relaxation theory, indicating that in the "extreme narrowing" cases $T_{1\rho}^{T,H}$ can be longer than $T_{1\rho}^{H}$. Table 1 lists the values of $T_{1\rho}^{H}$ and $T_{1\rho}^{T,H}$ at different RF spin-lock amplitudes in the

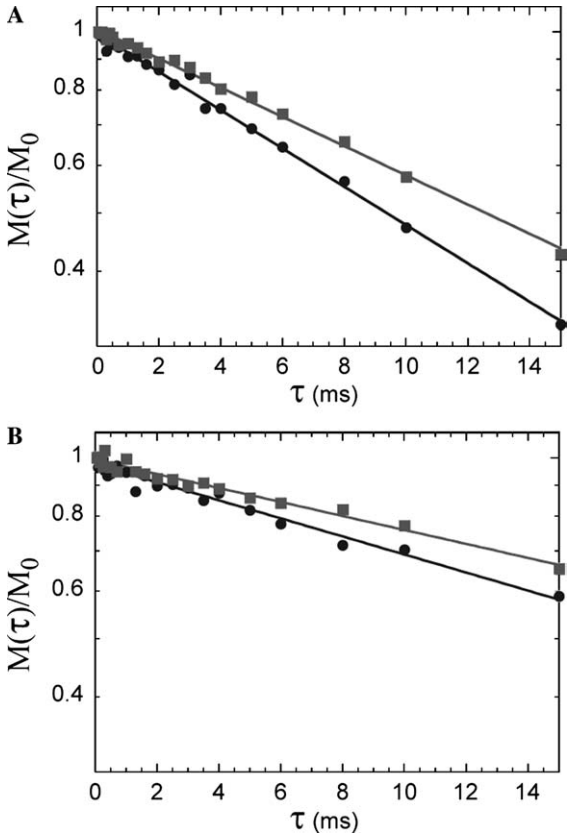

Fig. 3. Semilog plot of normalized magnetization intensities as a function of spin-lock time using the pulse sequences diagrammed in Fig. 2. In these experiments, a Bruker CPMAS double-resonance NMR probe with 4 mm rotors was used. The sample was packed into a 4 mm MAS rotor and was spun at 6.0 kHz to reduce spinning sideband intensities. A recycle delay of 10 s was used and τ_{CP} was set to 2 ms in the experiments. Experimental data are indicated by the solid circles and squares for the peaks positioned at 231.0 and 171.8 ppm, respectively. (A) Spin lock in the x–y plane where the ^{1}H RF spin-lock amplitude during the spin-lock time τ and contact time τ_{CP} was 50.0 kHz. The ^{1}H spin–lattice relaxation time $T_{1\rho}^{H}$ in the x–y plane obtained by fitting the experimental data, as indicated by the solid lines, was 13.63 and 17.88 ms for the resonance peaks at 231.0 and 171.8 ppm, respectively. (B) Spin lock at the magic angle where the ^{1}H RF amplitude during the spin lock time τ and the contact time τ_{CP} was 40.8 and 50.0 kHz, respectively, while the ^{1}H carrier frequency was switched to 28.9 kHz away from the center of the ^{1}H spectrum during the spin lock time but changed back to the center of the ^{1}H spectrum during the CP contact and decoupling periods. Therefore, the effective ^{1}H spin lock amplitude during the spin lock time was the same as in (A). The ^{1}H spin–lattice relaxation time $T_{1\rho}^{T,H}$ at the magic angle obtained by fitting the experimental data (solid lines) was 28.92 and 37.40 ms for the resonance peaks at 231.0 and 171.8 ppm, respectively.

x–y plane and at the magic angle. Clearly, higher ^{1}H RF spin-lock amplitude in the x–y plane does not necessarily increase the values of $T_{1\rho}^{H}$ but higher effective ^{1}H RF spin-lock amplitude along the magic angle prolongs the $T_{1\rho}^{T,H}$ values further.

Fig. 4 shows three CP pulse sequences where the RF amplitudes used to spin-lock ^{1}H and ^{15}N spins are rectangular but their carrier frequencies are different during the contact time. For conventional CWCP (cf.

Table 1
Proton spin–lattice relaxation time in the rotating frame of the two ^{15}N–δ_1-histidine species at different spin-lock amplitudes

Spin-lock amplitude (kHz)		38	50	57	67
$T_{1\rho}^{H}$ in the *xy* plane (ms)	Non-protonated ^{15}N (for species I)	13.15	13.63	14.49	14.50
	Protonated ^{15}N (for species III)	17.60	17.88	18.06	18.06
$T_{1\rho}^{T,H}$ at the magic angle (ms)	Non-protonated ^{15}N (for species I)	23.72	28.92	30.72	33.83
	Protonated ^{15}N (for species III)	32.80	37.40	39.85	41.02

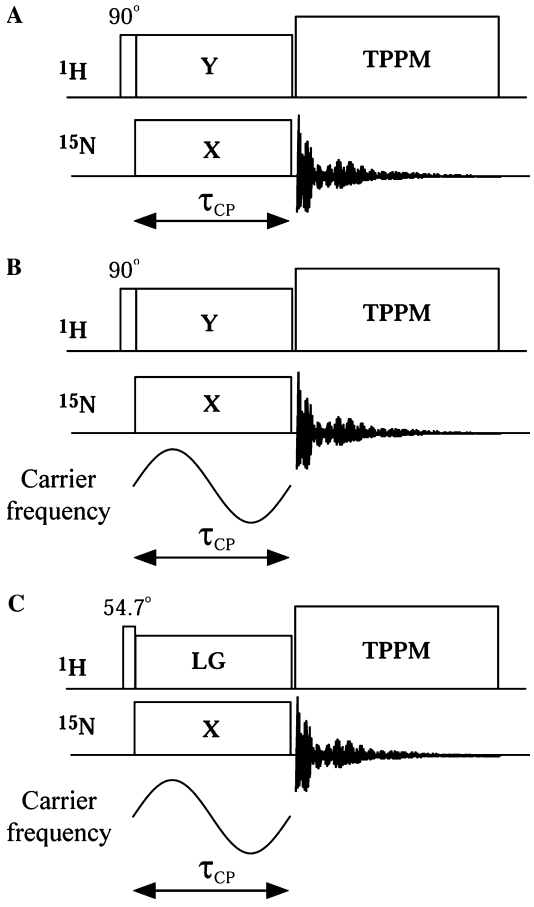

Fig. 4. Pulse sequences for cross-polarization with constant RF amplitudes used to transfer polarization from abundant ^1H spins to dilute ^{15}N spins. (A) CWCP, (B) CW-FMCP, and (C) LG-FMCP.

Fig. 4A), both the ^1H and ^{15}N spins are locked with two fixed RF carrier frequencies, normally positioned in the center of the ^1H and ^{15}N spectra, respectively. In Fig. 4B, the ^1H carrier frequency is applied in the center of the ^1H spectrum while the ^{15}N irradiation offset is modulated sinusoidally, as described in Eq. (1), during the contact time, τ_{CP}. The average of the frequency modulation is positioned in the center of the ^{15}N spectrum. In fact, this continuous-wave frequency modulated cross-polarization scheme is one of the frequency modulation schemes used to broaden the Hartmann–Hahn matching condition in the presence of fast MAS [20,32], and thus is dubbed CW-FMCP. In Fig. 4C, the ^1H carrier frequency is switched to an offset of $\Delta\omega_H = \omega_{1H}/\sqrt{2}$ away from the center of the ^1H spectrum for a period of τ_{CP} during which the ^{15}N irradiation offset is modulated in a sine wave, where ω_{1H} is the ^1H RF amplitude. Therefore, ^1H magnetization is flipped to the magic angle by a 54.7° pulse and then spin-locked along the magic angle by the LG sequence with the effective ^1H spin-lock amplitude of $\omega_{\text{eff }H} = \sqrt{3/2}\omega_{1H}$, as in Fig. 2B, thus resulting in a considerably longer $T_{1\rho}^{T,H}$. Since the CP occurs under the LG sequence (for ^1H) and frequency modulation (for ^{15}N), it is abbreviated as LG-FMCP.

Fig. 5 shows the ^{15}N CPMAS NMR spectra of the ^{15}N-δ_1-L-histidine sample at various contact times using the pulse sequences diagramed in Fig. 4. It can be seen from Figs. 5A, C, and E that at a contact time of 2 ms, both the CW-FMCP and LG-FMCP methods result in about 28% more signal intensity for the non-protonated ^{15}N (at 231.0 ppm) compared to the CWCP scheme, implying that the polarization buildup for the non-protonated ^{15}N is faster when the frequency modulation scheme is used. While for the protonated ^{15}N (at 171.8 ppm), the CWCP and CW-FMCP schemes generated the same signal intensity, the LG-FMCP method suffered about 20% signal loss compared to the other two methods. As the CP contact time increased from 2 to 8 ms, for the CWCP scheme, the non-protonated ^{15}N signal intensities increased by about 50%, but the protonated ^{15}N signal intensity decreased by as much as 20%. Similar behavior was also observed in Figs. 1B and C, though the percentages of the signal intensity variations were different, which is attributed to the effect of the sample spinning speed on CP dynamics and the differences in the RF spin-lock amplitudes. For CW-FMCP, the signal intensities for both the non-protonated and protonated ^{15}N were almost identical to that for CWCP (cf. Figs. 5B and D). Interestingly, for LG-FMCP, the non-protonated and protonated ^{15}N signal intensities were about 27 and 20% higher, respectively, than that obtained in the CWCP and CW-FMCP experiments at the same contact time of 8 ms. It is worth noting that the ^1H RF amplitude during the LG sequence was decreased to 40.8 kHz so that the effective ^1H spin-lock amplitude was kept the same as in CWCP and CW-FMCP. On the other hand, for both the frequency modulation schemes, the ^{15}N RF amplitude during the contact time was decreased to 31.0 from 50.0 kHz used

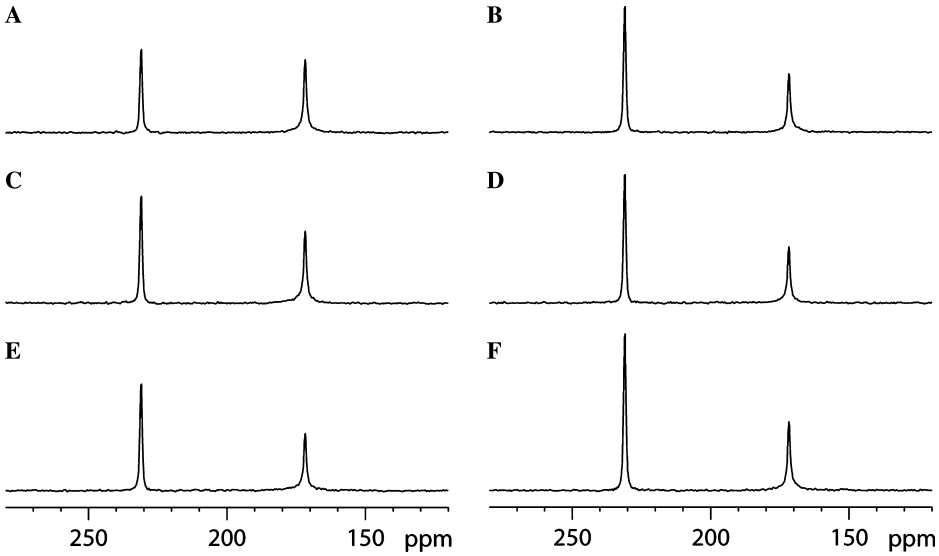

Fig. 5. ^{15}N CPMAS NMR spectra of the ^{15}N–δ_1-histidine sample recorded using various CP schemes as diagrammed in Fig. 4. Again in these experiments, a Bruker CPMAS double-resonance NMR probe with 4 mm rotors was used and the sample was spun at 6.0 kHz with a recycle delay of 10 s. Only the center-bands are shown in these spectra. (A) CWCP with a contact time of 2 ms. (B) CWCP with a contact time of 8 ms. (C) CW-FMCP with a contact time of 2 ms. (D) CW-FMCP with a contact time of 8 ms. (E) LG-FMCP with a contact time of 2 ms. (F) LG-FMCP with a contact time of 8 ms. For CWCP, both the ^{1}H and ^{15}N RF spin-lock amplitudes used during the contact time were 50.0 kHz. For CW-FMCP, the ^{1}H RF spin-lock amplitude during the contact time was kept 50.0 kHz while its CP matched ^{15}N RF amplitude became 31.0 kHz due to the frequency modulation. For LG-FMCP, during the contact time, the ^{1}H carrier frequency was switched to 28.9 kHz away from the center of the ^{1}H spectrum and its RF amplitude was decreased to 40.8 kHz so that the effective ^{1}H spin lock amplitude was 50.0 kHz, the same as in the CWCP and CW-FMCP experiments. The ^{15}N RF amplitude was set to 31.0 kHz for the best CP match condition.

in CWCP in order to obtain maximum polarization transfer.

Fig. 6 shows the ^{15}N integrated signal intensities (including all sideband intensities) as a function of CP contact time, τ_{CP}. Assuming that the spin–lattice relaxation time of the ^{15}N spins in the rotating frame $T_{1\rho}^S$ is long, the polarization buildup of the ^{15}N spins can be rationalized by the classical I–S model [10], as follows:

$$M(\tau_{CP}) = M_0 \exp\left(-\tau_{CP}/T_{1\rho}^H\right)/(1-\lambda) \times\{1-\exp[-(1-\lambda)\tau_{CP}/T_{NH}]\}, \quad (2)$$

where $\lambda = T_{NH}/T_{1\rho}^H$ and T_{NH} is the cross-polarization time between ^{1}H and ^{15}N spins. The experimental data were fitted using Eq. (2), as indicated by solid lines in Fig. 6A, where M_0 and T_{NH} were treated as variables and the values of $T_{1\rho}^H$ obtained from Fig. 3A were used as constants. The fitting yielded a T_{NH} value of 4100 ± 118 and 390 ± 27 μs for the non-protonated and protonated ^{15}N, respectively. In the system studied here, the T_{NH} value for the protonated ^{15}N was much shorter than the $T_{1\rho}^H$ value of 17.88 ms so that the polarization for the protonated ^{15}N increased rapidly to its maximum before $T_{1\rho}^H$ significantly reduced the polarization. However, for the non-protonated ^{15}N site the polarization buildup is more than ten times slower than that for the protonated ^{15}N site while the $T_{1\rho}^H$ value for the former one is smaller than for the latter one, so that the polarization for the non-protonated ^{15}N becomes proportionately less due to these competing effects. When the deviation of $M(\tau_{CP})$ in Eq. (2) becomes zero, the observable magnetization reaches its maximum, M_{obs}^{max}

$$M_{obs}^{max} = \xi M_0, \quad (3)$$

where, the weighting factor can be mathematically derived as $\xi = \lambda^{\lambda/(1-\lambda)}$. Apparently, the weighting factor ξ is decreased with an increase of λ value. In addition, as can be seen in Eq. (2), the polarization buildup rate $1/T_{NH}$ is scaled by a factor of $(1-\lambda)$ so that a large value of λ further decreases the rate of the polarization transfer. Therefore, polarized ^{15}N signal intensities can be sufficiently enhanced by shortening the T_{NH} value and/or lengthening the $T_{1\rho}^H$ value. For the non-protonated and protonated ^{15}N signals measured here, the weighting factor ξ was calculated to be 0.596 and 0.918, respectively.

For CW-FMCP, the classical I–S model (cf. Eq. (2)) was used to fit the experimental data, as indicated by the solid lines in Fig. 6B. The fittings yielded a T_{NH} value of 2871 ± 162 and 399 ± 19 μs for the non-protonated and protonated ^{15}N, respectively. Surprisingly, the value of T_{NH} for the protonated ^{15}N was virtually the same in both the CW-FMCP and CWCP schemes. However, the T_{NH} value for the non-protonated ^{15}N significantly decreased from 4100 μs in CWCP, implying that the polarization buildup for the non-protonated ^{15}N is faster in CW-FMCP than in CWCP. The weighting factor ξ became 0.660 and 0.918 for the non-protonated and

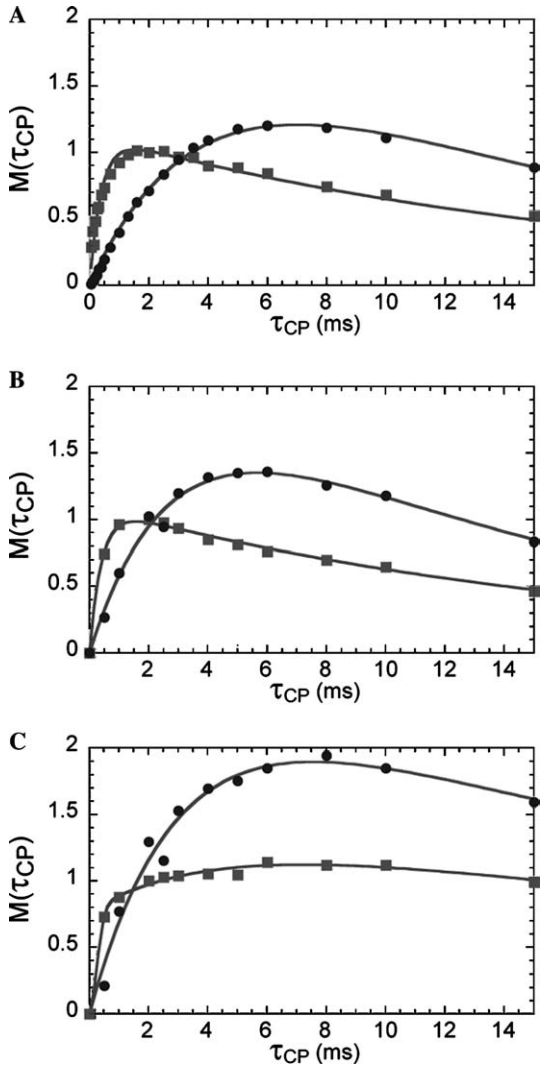

Fig. 6. Integrated ^{15}N signal intensities recorded as a function of contact time τ_{CP} using different CP schemes. All intensities were normalized to the integrated signal intensities at 171.8 ppm recorded by their respective CP schemes at a contact time of 2 ms. The solid circles and squares indicate the experimental data for the resonances at 231.0 and 171.8 ppm, respectively. (A) CWCP, (B) CW-FMCP, and (C) LG-FMCP.

protonated ^{15}N signals, respectively. In fact, it is evident that the non-protonated signal in Fig. 5C is about 28% higher than that in Fig. 5A at a contact time of 2 ms. However, as can be seen in Figs. 5B and D, although a longer contact time (e.g., 8 ms) enhanced the non-protonated ^{15}N signal further, it sacrificed the protonated ^{15}N signal because of the $T_{1\rho}^{H}$ effect.

Fig. 6C shows the ^{15}N polarization buildups under the LG-FMCP scheme. Since the non-protonated ^{15}N signal was cross-polarized from remote protons via weak heteronuclear dipolar interactions [17], Eq. (2) was used to fit the experimental data (solid circles) where $T_{1\rho}^{H}$ is simply replaced by $T_{1\rho}^{T,H}$, resulting in a T_{NH} value of 2981 ± 238 μs, which is within the error bar for that obtained by CW-FMCP and much smaller than that obtained by CWCP. Clearly, this observation indicates that the direction of the ^{1}H spin-lock field has little effect on the cross-polarization time T_{NH}, even if the ^{1}H off-resonance spin-lock scales the heteronuclear ^{1}H-^{15}N dipolar coupling. In fact, the rate of the polarization buildup can be rationalized by [4,12]

$$\frac{1}{T_{NH}} \propto \frac{M_{2,NH}}{\sqrt{M_{2,HH}}}, \tag{4}$$

where $M_{2,NH}$ and $M_{2,HH}$ are the second moments, which reflect the ^{15}N–^{1}H and ^{1}H–^{1}H dipolar couplings, respectively. The LG sequence scales the ^{15}N–^{1}H dipolar coupling by a factor of 0.57 so that the second moment $M_{2,NH}$ is reduced accordingly. However, the LG sequence also removes the ^{1}H homonuclear dipolar coupling to the first order and attenuates the proton second moment $M_{2,HH}$. Therefore, the overall effect on the rate of the polarization buildup could become rather small. Because the value of $T_{1\rho}^{T,H}$ for the non-protonated ^{15}N site was significantly increased by the LG sequence, the weighting factor ξ for the non-protonated ^{15}N signal has become 0.770, much larger than that for CWCP and CW-FMCP. Therefore, lengthening $T_{1\rho}^{T,H}$ not only minimizes the proton relaxation effect on the ^{15}N polarization buildup, but also increases the weighting factor ξ, thus effectively reducing the rate of the ^{15}N polarization buildup and increasing the polarization intensity as well.

For the protonated ^{15}N, the *I-I*-S* CP model [33,34] should be used to describe the CP dynamics due to the fact that the ^{1}H–^{1}H homonuclear dipolar coupling is largely attenuated by the LG sequence, where the asterisk denotes protons in close proximity to the ^{15}N, as formulated in the following [35]:

$$M(\tau_{CP}) = M_0 \exp\left(-\tau_{CP}/T_{1\rho}^{T,H}\right) \times \left[1 - \frac{1}{2}\exp(-\tau_{CP}/T_{df}) - \frac{1}{2}\exp(-1.5\tau_{CP}/T_{df}) \times \exp\left(-0.5\tau_{CP}^2/T_2^2\right)\right], \tag{5}$$

where, T_{df} refers to the proton spin diffusion constant and the decay rate of $1/T_2$ may be considered as a root-mean-square average of the heteronuclear dipolar couplings weighted by the fraction of $I^*/\Sigma_i I_i$ over all orientations. Again, with the measured $T_{1\rho}^{T,H}$ of 37.4 ms as a constant, the experimental data (solid squares) were fitted using Eq. (5), resulting in T_{df} of 5004 ± 836 and T_2 of 261 ± 19 μs, as indicated by the solid line in Fig. 6c. In Lee–Goldburg cross-polarization experiments [36,37], the polarization buildup is in an oscillatory manner corresponding to the heteronuclear dipolar coupling constant owing to the use of a sideband of the Hartmann–Hahn match condition. However, such a time-oscillatory buildup is not apparent in our LG-FMCP experiments because FMCP fulfills the adiabatic cross-

polarization condition [20,32]. It was known that the adiabatic passage Hartmann–Hahn condition could lead to negligible transient oscillations [38]. As seen in Fig. 6C, the ^{15}N polarization buildup can be rationalized in three stages. In the first 500 μs or so, the ^{15}N signal increases rapidly with a time constant of T_2, which is similar to T_{NH} in the CWCP and CW-FMCP schemes, and then slowly gains more intensity with a time constant of T_{df}. Finally, the decay of the ^{15}N signal due to $T_{1\rho}^{T,H}$ becomes apparent. Since $T_{1\rho}^{T,H}$ along the magic angle is much longer than T_{df}, the $T_{1\rho}^{H}$ effect is very small at a relatively short CP contact time. As can be seen in Fig. 5f, the protonated ^{15}N signal intensity at a contact time of 8 ms is almost the same as the maximum polarized ^{15}N signal obtained at a contact time of 2 ms by using the CWCP scheme (cf. Fig. 5A). Therefore, with a relatively long CP contact time (e.g., 8 ms), LG-FMCP allows one to obtain nearly maximal signals for both protonated and non-protonated ^{15}N.

As an example, Fig. 7 shows the ^{15}N CPMAS spectra of ^{15}N–δ_1-His_{37} labeled transmembrane peptide of the M2 protein in hydrated DMPC/DMPG bilayers at pH 8.8 recorded at 277 K with the CWCP and LG-FMCP schemes. Again, the resonance at 231 ppm is from the neutral species (I) and the broad peak at 147 ppm is assigned to the protonated ^{15}N signals resulting from the neutral species (II) [24]. The signal at around 100 ppm stems from the natural abundant ^{15}N peptide bonds. The rate of the polarization buildup for the non-protonated ^{15}N is so slow that there is a need to use a relatively long contact time (e.g., 3 ms) to polarize the non-protonated ^{15}N signal of species (I), although the maximum signal intensity for the protonated ^{15}N was achieved at a contact time of 1 ms. However, the value of $T_{1\rho}^{H}$ in the hydrated peptide sample is on the order of a few milliseconds [17,29] so that even a 3 ms contact time results in a significant attenuation of the protonated ^{15}N signal intensity, as shown in Fig. 7A. In contrast, by lengthening $T_{1\rho}^{T,H}$ LG-FMCP dramatically improves the protonated ^{15}N signal intensity while slightly increases the non-protonated ^{15}N signal intensity, as illustrated in Fig. 7B.

For both CWCP and CW-FMCP, the protonated ^{15}N signal from the amino acid powder reached its maximum at a contact time of 2 ms, while the maximum non-protonated ^{15}N signal intensity was achieved at a contact time of ~6 ms. Optimal CP contact time for accurate quantitation with CWCP and CW-FMCP is at 10 ms or more where signal intensities are only 72% of the intensities achieved with LG-FMCP, where it is optimized for quantitation at 8 ms. In the amino acid sample studied here, the sums of the non-protonated and protonated ^{15}N signals reached a maximum at a contact time of 5 and 4 ms for CWCP and CW-FMCP, respectively. Even these maximal values represented only 84 and 88% of the signal intensities obtained with LG-FMCP at 8 ms. Table 2 lists the population ratios of the two ^{15}N–δ_1-histidine species calculated from the ^{15}N MAS NMR spectra obtained with those contact times.

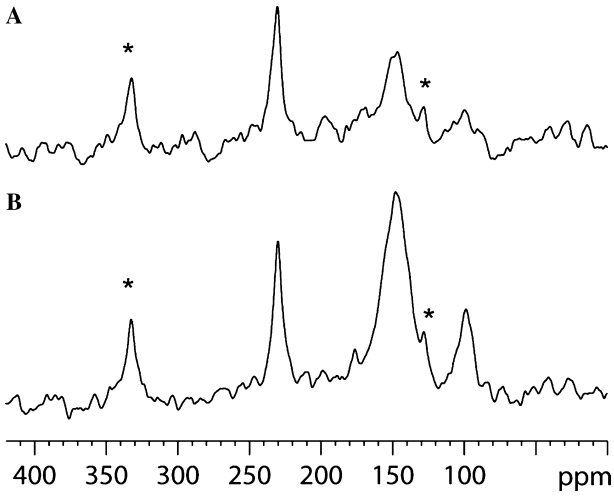

Fig. 7. ^{15}N CPMAS NMR spectra of ^{15}N–δ_1-His_{37} transmembrane peptide of the M2 protein in unoriented hydrated DMPC/DMPG bilayers at pH 8.8 recorded at 277 K using different CP schemes. A Bruker CPMAS NMR probe with 7 mm rotors was used in the experiments. The sample was packed into a 7 mm MAS rotor and was spun at 3.1 kHz during the measurements. The CP contact time used was 3 ms. 15,000 scans were used for signal accumulation with a recycle delay of 6 s. (A) CWCP. The ^{1}H RF spin-lock amplitude was set to 27.8 kHz and the ^{15}N RF spin-lock amplitude was 22.7 kHz. (B) LG-FMCP. The ^{1}H RF spin-lock amplitude was set to 22.7 kHz and its carrier frequency was switched to 16.1 kHz away from the center of the ^{1}H spectrum during the contact time. While the ^{15}N RF spin-lock amplitude was 18.0 kHz and the depth of the frequency modulation was 50 kHz. The asterisks indicate the spinning sidebands.

Table 2
Population ratio of the two ^{15}N–δ_1-histidine species calculated from ^{15}N NMR spectra recorded using different experimental schemes

Experimental scheme	BD	CWCP			CW-FMCP			LG-FMCP
		2 ms[a]	5 ms[b]	6 ms[c]	2 ms[a]	4 ms[b]	6 ms[c]	8 ms[a,b,c]
Species I vs. Species III	1.94	0.71	1.32	1.43	1.02	1.55	1.78	1.74
% of maximum intensity[d]		70	84	83	83	88	86	100

[a] A contact time (CT) used to obtain the maximum protonated ^{15}N signal intensity.
[b] A CT to achieve the maximum ^{15}N polarization (i.e., a combined intensity of the protonated and non-protonated ^{15}N signals).
[c] A CT for the maximum non-protonated ^{15}N signal intensity.
[d] A percentage of the combined intensity of the protonated and non-protonated signals compared to that obtained by LG-FMCP at an 8 ms CT.

Clearly, with a contact time of 2 ms, the ratio obtained in either the CWCP or CW-FMCP scheme is much smaller than that in the BD experiment and the value of the ratio increases as the contact time becomes longer at the expense of the protonated ^{15}N sensitivity. However, for LG-FMCP both the non-protonated and protonated ^{15}N signals reached their maximal values at the same contact time of 8 ms. Therefore, it appears that a contact time can be chosen in practice by maximizing signals for different structural groups using LG-FMCP. With an 8 ms contact time, the population ratio calculated from the resulting LG-FMCP spectrum was 1.74, about 10% lower than that in the BD experiment.

Theoretically, quantitative CP measurements can be achieved at a relatively long contact time while maintaining maximal spectral intensities only when the ^{1}H spin–lattice relaxation effect becomes negligible, i.e., $T_{1\rho}^{T,H}$ or $T_{1\rho}^{T,H} \gg T_{IS}$. For systems where $T_{1\rho}^{H}$ is comparable with, or shorter than, the cross-polarization time T_{IS}, such as the membrane proteins in hydrated lipid bilayers, cross-polarized signal intensities are greatly attenuated by the proton relaxation effect. By spin-locking the ^{1}H magnetization along the magic angle, $T_{1\rho}^{T,H}$ can be significantly lengthened. In addition, the cross-polarization time T_{IS} is also greatly shortened by the frequency modulation. Consequently, LG-FMCP not only greatly enhances the polarized signal intensities but also increases the probability to fulfill the condition of $T_{1\rho}^{T,H} \gg T_{\mathrm{IS}}$. In case that $T_{1\rho}^{T,H}$ is still comparable with, or shorter than, T_{IS}, the quantitation may have to be obtained by combining LG-FMCP with variable contact time CP experiments [15,16]. For dilute nuclei with higher gyromagnetic ratios such as ^{13}C this may be relatively easy to accomplish because the nuclei with higher gyromagnetic ratios exhibit stronger dipolar couplings with protons and typically give rise to a shorter value of T_{IS}. It is worth noting that, due to the frequency modulation, the ^{15}N RF amplitude during the contact time was decreased to 31.0 kHz in order to match the effective ^{1}H RF spin-lock amplitude of 50 kHz for maximizing ^{15}N polarization. Since higher effective ^{1}H RF spin-lock amplitude at the magic angle can lengthen the values of $T_{1\rho}^{T,H}$, it would be preferable to perform the LG-FMCP experiments at higher RF amplitudes so as to further minimize the $T_{1\rho}^{T,H}$ effect on the CP dynamics and to increase the weighting factor.

4. Conclusion

We have demonstrated that Lee–Goldburg frequency modulated cross-polarization (LG-FMCP) provides an efficient means for polarizing dilute S spins from protons, especially for those weakly coupled to protons. Frequency modulation on the S channel greatly shortens the cross-polarization time for the non-protonated S spins, but has a limited effect on polarization buildup of the protonated S spins. Spin-locking ^{1}H magnetization at the magic angle by the LG sequence significantly prolongs the proton spin–lattice relaxation time in the tilted rotating frame $T_{1\rho}^{T,H}$. Although the LG sequence scales the heteronuclear dipolar interaction, it has very little effect on the cross-polarization time for the non-protonated S spins. A long $T_{1\rho}^{T,H}$ not only minimizes the deleterious effect of proton decay on polarization transfer, but also increases the weighting factor, thus allowing one to more efficiently polarize the non-protonated S spins with a relatively long CP contact time without sacrificing the polarization of the protonated S spins. Importantly, the contact time for achieving the most accurate assessment of relative intensities is when the individual intensities are maximized in the LG-FMCP experiment, in sharp contrast to CWCP and CW-FMCP. Not only is this true for the amino acid sample used here, but also this amino acid incorporated into a peptide and characterized in hydrated lipid bilayers, two situations with very different dynamics. Consequently, the LG-FMCP experiment enhances the probability for achieving more accurate relative intensities in cross-polarized solid-state NMR spectra.

Acknowledgments

This work was supported in part by the National Science Foundation MCB 02-35774 and the work was performed at the National High Magnetic Field Laboratory supported by the National Science Foundation Cooperative Agreement DMR-0084173 and the State of Florida. We are indebted to Prof. John S. Waugh for useful discussion about the proton spin–lattice relaxation in the tilted rotating frame and to referees for thoughtful comments.

References

[1] D.M. Kushlan, D.M. LeMaster, Resolution and sensitivity enhancement of heteronuclear correlation for methylene resonances via ^{2}H enrichment and decoupling, J. Biomol. NMR 3 (1993) 701–708.
[2] T. Yamazaki, W. Lee, C.H. Arrowsmith, D.R. Muhandiram, L.E. Kay, A suite of triple resonance NMR experiments for the backbone assignment of ^{15}N, ^{13}C, ^{2}H labeled proteins with high sensitivity, J. Am. Chem. Soc. 116 (1994) 11655–11666.
[3] C.H. Wu, A. Ramamoorthy, S.J. Opella, High-resolution heteronuclear dipolar solid-state NMR spectroscopy, J. Magn. Reson. Ser. A 109 (1994) 270–272.
[4] A. Pines, M.G. Gibby, J.S. Waugh, Proton-enhanced NMR of dilute spins in solids, J. Chem. Phys. 59 (1973) 569–590.
[5] S.R. Hartmann, E.L. Hahn, Nuclear double resonance in the rotating frame, Phys. Rev. 128 (1962) 2042–2053.
[6] E.O. Stejskal, J. Schaefer, J.S. Waugh, Magic-angle spinning and polarization transfer in proton-enhanced NMR, J. Magn. Reson. 28 (1977) 105–112.

[7] M. Sardashti, G.E. Maciel, Effects of sample spinning on cross polarization, J. Magn. Reson. 72 (1987) 467.
[8] D.A. McArthur, E.L. Hahn, Rotating-frame nuclear-double-resonance dynamics: dipolar fluctuation spectrum in CaF_2, Phys. Rev. 188 (1969) 609–638.
[9] D.E. Demco, J. Tegenfeldt, J.S. Waugh, Dynamics of cross polarization in nuclear magnetic double resonance, Phys. Rev. B 11 (1975) 4133–4151.
[10] M. Mehring, Principles of High Resolution NMR in Solids, second ed., Springer-Verlag, New York, 1983.
[11] W. Kolodziejski, J. Klinowski, Kinetics of cross-polarization in solid-state NMR: a guide for chemists, Chem. Rev. 102 (2002) 613–628.
[12] C. Fuelber, D.E. Demco, B. Bluemich, The influence of molecular motion on cross polarization in cross-linked elastomers, Solid State Nucl. Magn. Reson. 6 (1996) 213–223.
[13] M. Geppi, F. Ciardelli, C.A. Veracini, C. Forte, G. Cecchin, P. Ferrari, Dynamics and morphology of polyolefinic elastomers by means of ^{13}C and ^{1}H solid-state NMR, Polymer 38 (1997) 5713–5722.
[14] I. Ando, M. Kobayyashi, M. Kanekiyo, S. Kuroki, S. Ando, S. Matsukawa, H. Kurosu, H. Yasunaga, S. Amiya, NMR spectroscopy in polymer science, in: T. Tanaka (Ed.), Experimental Methods in Polymer Science: Modern Methods in Polymer Research and Technology, Academic Press, London, 2000, pp. 261–493.
[15] M.S. Solum, R.J. Pugmire, D.M. Grant, ^{13}C solid-state NMR of Argonne premium coals, Energy Fuels 3 (1989) 187–193.
[16] M.A. Wilson, NMR Techniques and Applications in Geochemistry and Soil Chemistry, Pergamon Press, Oxford, England, 1987.
[17] F. Tian, T.A. Cross, Dipolar oscillations in cross-polarized peptide samples in oriented lipid bilayers, J. Magn. Reson. 125 (1997) 220–223.
[18] W. Kolodziejski, J. Klinowski, $^{13}C \rightarrow {}^{1}H \rightarrow {}^{13}C$ cross polarization NMR in toluene-solvated fullerene-70, Chem. Phys. Lett. 247 (1995) 507–509.
[19] W. Kolodziejski, A. Corma, K. Wozniak, J. Klinowski, $^{13}C \rightarrow {}^{1}H$ cross polarization NMR in solids at natural ^{13}C abundance, J. Phys. Chem. 100 (1996) 7345–7351.
[20] R. Fu, P. Pelupessy, G. Bodenhausen, Frequency-modulated cross-polarization for fast magic angle spinning NMR at high field: relaxing the Hartmann–Hahn condition, Chem. Phys. Lett. 264 (1997) 63–69.
[21] A.E. Bennett, C.M. Rienstra, M. Auger, K.V. Lakshmi, R.G. Griffin, Heteronuclear decoupling in rotating solids, J. Chem. Phys. 103 (1995) 6951–6958.
[22] F. Kovacs, T.A. Cross, Transmembrane four-helix bundle of Influenza A M2 protein channel: structural implications from helix tilt and orientation, Biophys. J. 73 (1997) 2511–2517.
[23] K. Nishimura, S. Kim, L. Zhang, T.A. Cross, The closed state of a H^+ channel helical bundle combining precise orientational and distance restraints from solid state NMR, Biochemistry 41 (2002) 13170–13177.
[24] M. Munowitz, W.W. Bachovchin, J. Herzfeld, C.M. Dobson, R.G. Griffin, Acid–base and tautomeric equilibria in the solid state: ^{15}N NMR spectroscopy of histidine and imidazole, J. Am. Chem. Soc. 104 (1982) 1192–1196.
[25] B. Henry, P. Tekely, J.J. Delpuech, pH and *p*K determinations by high-resolution solid-state ^{13}C NMR: acid–base and tautomeric equilibria of lyophilized L-histidine, J. Am. Chem. Soc. 124 (2002) 2025–2034.
[26] Y. Wei, A.C. de Dios, A.E. McDermott, Solid-state ^{15}N NMR chemical shift anisotropy of histidines: experimental and theoretical studies of hydrogen bonding, J. Am. Chem. Soc. 121 (1999) 10389–10394.
[27] F. Bloch, Nuclear induction, Phys. Rev. 70 (1946) 460–474.
[28] M. Lee, W. Goldburg, Nuclear magnetic resonance line narrowing by a rotating RF field, Phys. Rev. 140 (1965) 1261–1271.
[29] R. Fu, C. Tian, T.A. Cross, NMR spin locking of proton magnetization under frequency switched Lee–Goldburg (FSLG) pulse sequence, J. Magn. Reson. 154 (2002) 130–135.
[30] P. Tekely, P. Palmas, D. Canet, Effect of proton spin exchange on the residual ^{13}C MAS NMR linewidth. Phase-modulated irradiation for efficient heteronuclear decoupling in rapidly rotating solids, J. Magn. Reson. Ser. A 107 (1994) 129–133.
[31] U. Haeberlen, J.S. Waugh, Spin-lattice relaxation in periodically perturbed systems, Phys. Rev. 185 (1969) 420–429.
[32] A.C. Kolbert, A. Bielecki, Broadband Hartmann–Hahn matching in magic-angle spinning NMR via an adiabatic frequency sweep, J. Magn. Reson. Ser. A 116 (1995) 29–35.
[33] L. Müller, A. Kumar, T. Baumann, R.R. Ernst, Transient oscillations in NMR cross-polarization experiments in solids, Phys. Rev. Lett. 32 (1974) 1402–1406.
[34] M.H. Levitt, D. Suter, R.R. Ernst, Spin dynamics and thermodynamics in solid-state NMR cross polarization, J. Chem. Phys. 84 (1986) 4243–4255.
[35] L.B. Alemany, D.M. Grant, T.D. Alger, R.J. Pugmire, Cross polarization and magic angle sample spinning NMR spectra of model organic compounds. 3. Effect of the ^{13}C–^{1}H dipolar interaction on cross polarization and carbon–proton dephasing, J. Am. Chem. Soc. 105 (1983) 6697–6704.
[36] B.-J. van Rossum, C.P. de Groot, V. Ladizhansky, S. Vega, H.J.M. de Groot, A method for measuring heteronuclear (^{1}H–^{13}C) distances in high speed MAS NMR, J. Am. Chem. Soc. 122 (2000) 3465–3472.
[37] V. Ladizhansky, S. Vega, Polarization transfer dynamics in Lee–Goldburg cross polarization under magnetic resonance experiments on rotating solids, J. Chem. Phys. 112 (2000) 7158–7168.
[38] S. Hediger, B.H. Meier, N.D. Kurur, G. Bodenhausen, R.R. Ernst, NMR cross polarization by adiabatic passage through the Hartmann–Hahn condition (APHH), Chem. Phys. Lett. 223 (1994) 283–288.